KFUPM
Journal of Undergraduate Research International

Diamond Open Access 43

Article Chemistry

Development of Sustainable Co–Red Mud Catalysts for Hydrogen Production via Steam Methane Reforming

Dana Alkhalifah and Aasif Helal*

Cite https://doi.org/10.64589/juri/231546

Submitted: April 18, 2026 Revised: May 13, 2026 Accepted: May 15, 2026

ABSTRACT

The growing demand for sustainable hydrogen production has increased interest in developing efficient, low-cost catalysts. However, the use of red mud as a catalyst support and the influence of cobalt loading on catalyst performance remain underexplored. In this study, cobalt–red mud (Co@RM) catalysts (with 5–20-wt.% cobalt loading) were synthesized via the wet impregnation method followed by high-temperature calcination and subjected to methane steam reforming (SMR) testing. Red mud, which is present in industrial waste, and which constitutes a potent source of iron, was used as a green catalyst support. The synthesized catalysts were examined via X-ray diffraction analysis, Fourier-transform infrared spectroscopy, thermogravimetric analysis, transmission electron microscopy, and scanning electron microscopy. The results revealed the formation of Co_3O_4 and Co–Fe mixed oxide phases while the structural integrity of the red-mud support was maintained. The catalytic performance indicated effective methane conversion and hydrogen production: for 5% Co@RM, the methane conversion rate reached up to 96.9% with a hydrogen yield of approximately 50% under the test conditions. Additionally, a methane conversion rate exceeding 99% for more than 4 h was observed for the 10% Co@RM sample, indicating strong catalytic activity and resistance to deactivation. These results were attributed to the enhanced dispersion of the Co species on the red-mud surface and the formation of active metal–support interaction sites that promoted methane activation and reforming reactions. Overall, the Co@RM catalyst system examined in this study exhibits high SMR activity and stability, highlighting its potential as a low-cost and sustainable catalyst for hydrogen production.

Keywords: Hydrogen production, Steam methane reforming, red mud, cobalt catalyst, net-zero emission

1. INTRODUCTION

The global energy demand has increased significantly owing to the growth of the global population and the corresponding expansion of industrialization [1–3]. Although fossil fuels have traditionally served as the primary energy sources, their use has devastating environmental consequences, such as increased CO_2 emissions, which contribute to global warming and climate change [4–6]. Consequently, clean, renewable, and sustainable energy technologies to satisfy the ever-increasing demand for energy with minimal risk to the environment are required.

Hydrogen can be used as a fuel, energy carrier, and storage medium, thereby playing a critical role in the transition toward low-carbon energy systems [7–15]. CH_4 is the most widely used industrial precursor owing to its high hydrogen content and broad availability [4,5]. Steam methane reforming (SMR) is the primary industrial methane conversion process, and is responsible for ~48% of the current global hydrogen production [7]. The SMR process requires elevated temperature (700–1000 °C) and moderate pressure (3–30 bar) under which, the CH_4 reacts with steam over a suitable catalyst to produce H_2 (Eq. 1). The reactions are endothermic and followed by a water–gas shift reaction, in which CO is converted to CO_2 and more hydrogen is produced (Eq. 2).

$$CH_4 + H_2O \rightarrow CO + 3H_2 \quad \Delta H_1 = +206\,kJ/mol \qquad (1)$$

$$CO + H_2O \rightarrow CO_2 + H_2 \quad \Delta H_2 = -41\,kJ/mol \qquad (2)$$

Despite the high efficiency and industrial applicability of SMR, deactivation remains a critical challenge [10,11]. The commonly observed deactivation mechanisms are sintering, coking, thermal degradation, and poisoning [16–18]. Red mud (RM), a highly alkaline byproduct of alumina (bauxite) refining, has attracted attention as a cost-effective and sustainable support for reforming catalysts. The RM comprises Fe_2O_3, Al_2O_3, SiO_2, TiO_2, and alkali elements, which promote carbon gasification, catalytic activity, suppress coking, and improve resistance to sintering [19–21].

The performance of a catalyst strongly depends on its preparation method, metal loading, and support morphology [22]. Recently, the steam reforming of dodecane over an Ni–RM catalyst demonstrated hydrogen selectivity of 75% with stable performance for 20 h owing to enhanced Ni dispersion and strong metal–support interaction, while Co–Ni bimetallic catalysts exhibited CH_4 conversions of approximately 77.9% because

Published under an exclusive license by KFUPM

of stronger metal–support interactions and improved resistance to carbon formation [23,24]. Co-based catalysts supported on $MgAl_2O_4$ have also exhibited high activity attributed to well-dispersed Co species and strong metal–support interactions [25].

Co-doped RM has attracted attention because RM functions as a waste-derived support with structural stability, iron-based phases, and resistance to sintering and carbon deposition, whereas Co serves as the active metal for methane activation and hydrogen production in SMR. However, studies on Co–RM (Co@RM) catalysts for SMR remain limited, and the effect of Co loading on catalytic activity, stability, and resistance to carbon deposition is not yet fully understood [26]. Additionally, the utilization of industrial waste-derived materials, such as RM, as catalyst supports remains underexplored [27,28].

Therefore, this study systematically investigates the effect of Co loading on Co@RM catalyst performance, and confirms a clear relationship between the composition, structure, and activity. Co@RM catalysts with different Co loadings (0%, 5%, 10%, 15%, and 20%) are prepared for SMR, and their catalytic activity, stability, and deactivation resistance are tested in a realistic reaction environment. The novelty of this study is the use of RM as a waste-derived and low-cost support, and Co as a low-cost active metal, to obtain a sustainable and cost-efficient catalyst system. Furthermore, the proposed Co@RM catalysts constitute a novel solution that supports integrated industrial-waste treatment and carbon-emission reduction via clean hydrogen generation.

2. METHODOLOGY

2.1. Materials. RM (Maaden Mining Company, Ras Al Khair, Saudi Arabia) was used as the primary raw material. Analytical-grade hydrochloric acid (HCl, 37%, Fisher Scientific), ammonia solution (NH_3, 30%, Panreac), and cobalt (II) acetate tetrahydrate ($Co(CH_3COO)_2 \cdot 4H_2O$, Merck) were also employed, along with double-distilled deionized water filtered through a Millipore membrane system.

2.2. Preparation of Co@RM Catalyst. The RM was initially subjected to chemical treatment to improve its surface properties and suitability as a catalyst support. The process involved acid leaching with HCl to eliminate soluble impurities and undesired metallic elements. Upon leaching, the suspension was neutralized through the controlled addition of an aqueous ammonia solution to reach a pH of ~7. Before further treatment, RM neutralization was performed to remove the residual acidity and stabilize the treated RM. The neutralized RM was then filtered and washed with a sufficient quantity of deionized water to remove the free ions. The treated material was dried and then calcined in air at 950 °C for 3 h; this step was performed to enhance the thermal stability of the RM and induce structural modifications for catalyst support applications.

The Co-supported catalysts were prepared via the wet impregnation technique, with $Co(CH_3COO)_2 \bullet 4H_2O$ as the cobalt precursor. Aqueous solutions of the precursors were prepared for Co loadings of 5, 10, 15 and 20 wt.%. The appropriate amount of Co salt was dissolved in distilled water under stirring until complete homogenization was achieved. The calcined RM support was then impregnated with the prepared solutions and dried in oven at 120 °C for 24 hours. Hence, the final Co@RM catalysts were obtained; these catalysts were subsequently subjected to characterization and catalytic performance testing.

2.3. Characterization of Co@RM catalyst. The chemical compositions and morphologies of the synthesized catalysts were characterized using several techniques. Specifically, X-ray diffraction (XRD) was used to determine the crystalline phases of both the treated RM support and Co@RM catalysts, and to obtain phase composition information using a Rigaku MiniFlex diffractometer (Rigaku, Japan). Fourier-transform infrared spectroscopy (FTIR) analysis was conducted to study the surface functional groups and identify the interactions between the Co species and RM support using a Nicolet 6700 spectrometer (Thermo Scientific, USA). Thermogravimetric analysis (TGA) was performed to assess the thermal stability of the catalysts and the weight changes related to the decomposition of the precursors or adsorbed species using a TA Q500 thermogravimetric analyzer (TA Instruments, USA). Additionally, transmission electron microscopy (TEM) was used to study the morphology, size distribution, and dispersion of the Co nanoparticles on the RM support. High-resolution transmission electron microscopy (HRTEM) images were recorded using a JEOL JEM-2100F transmission electron microscope (JEOL, Japan). Prior to analysis, the samples were dispersed in ethanol to form a homogeneous suspension, deposited onto a copper grid, and dried at room temperature. Finally, the surface morphologies and topographical changes in the catalysts were studied using a field emission scanning electron microscope (FESEM, LYRA 3 Dual Beam, Tescan, Czech Republic). Energy-dispersive X-ray spectroscopy (EDS) was used to determine the elemental composition and elemental distribution of the catalysts. Gas chromatography (GC-2030, Shimadzu, Japan), equipped with a thermal conductivity detector (TCD) and a flame ionization detector (FID), was used to analyze and quantify the reaction products. These combined characterization techniques supported understanding of the structure, chemistry, and morphology of each of the Co–RM catalysts, providing knowledge that is critical for linking their properties to the catalytic performance observed in SMR.

3. RESULTS AND DISCUSSION

3.1. Characterization. The XRD patterns for RM and Co@RM (5–20%) recorded over 20–80°(2θ) confirmed the crystalline nature of the materials (Figure 1). The RM pattern was dominated by reflections at approximately 33°(104), 35.6°(110), 49.5°(024), and 63°(214); these results are characteristic of hematite (Fe_2O_3) and confirm iron oxide as the dominant crystalline phase. A clear peak at approximately 26.6°(101) was observed, which corresponds to SiO_2 (quartz). Although they were partially overlapped by iron-oxide reflections, weak peaks were found at 30°and 43°; these peaks are related to Ca-containing phases.

With Co incorporation into the RM, new and enhanced reflections were observed at approximately 30°(220), 43°(400), 53°(422), 57°(511), and 63°(440). These reflections correspond to cobalt ferrite ($CoFe_2O_4$) and indicate the formation of spinel-type structures due to solid-state interaction between the Co species and iron framework during calcination. A reflection at

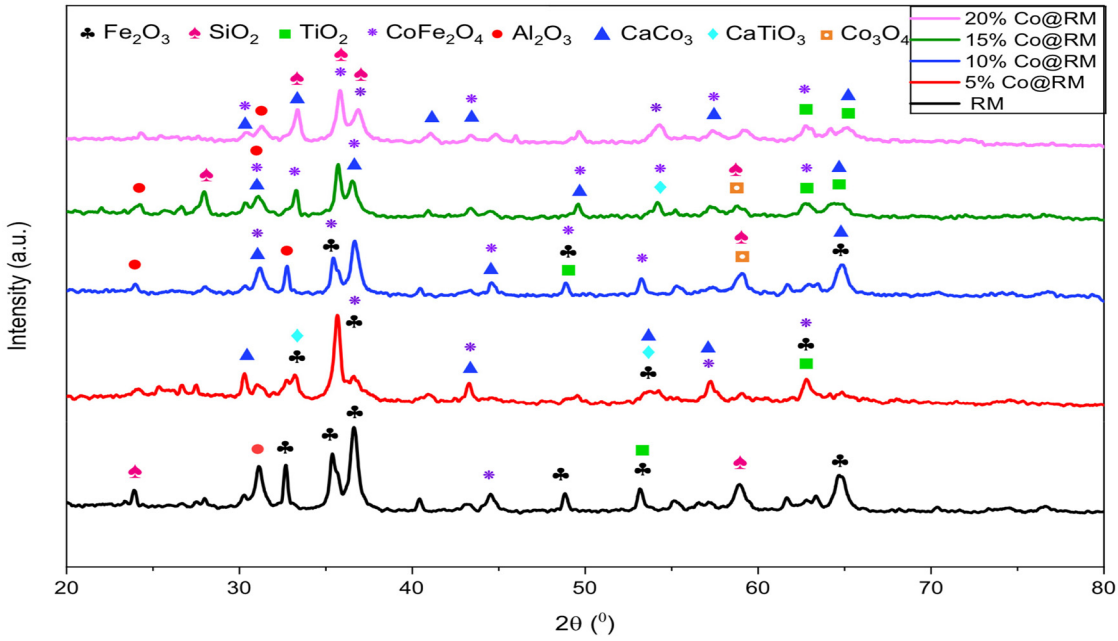

Figure 1. Powder XRD results for Co@RM (5, 10, 15, and 20%) catalysts

35–36°(311) was observed, which was enhanced by the Co loading; this region corresponds to overlapping contributions from hematite and cobalt ferrite, and the observed reflection suggests strong structural interaction rather than phase separation.

With increased Co loading (5–20%), a decrease in the diffraction peak intensity was observed; however, the peak broadening remained essentially constant. This suggests that the crystallinity and crystallite size of the Co-containing phases remained unchanged, and that the reduced intensity may be attributed to changes in phase distribution, dispersion, or interaction with the support. The main hematite and quartz reflections were still present; however, the change in their relative intensities within 30°–63°indicated a progressive modification of the phase composition, whereas the base RM structure remained intact. This structural evolution shows that the Co content directly governs the phase composition and crystallographic order, which are expected to influence the redox behaviors of Co–RM catalysts.

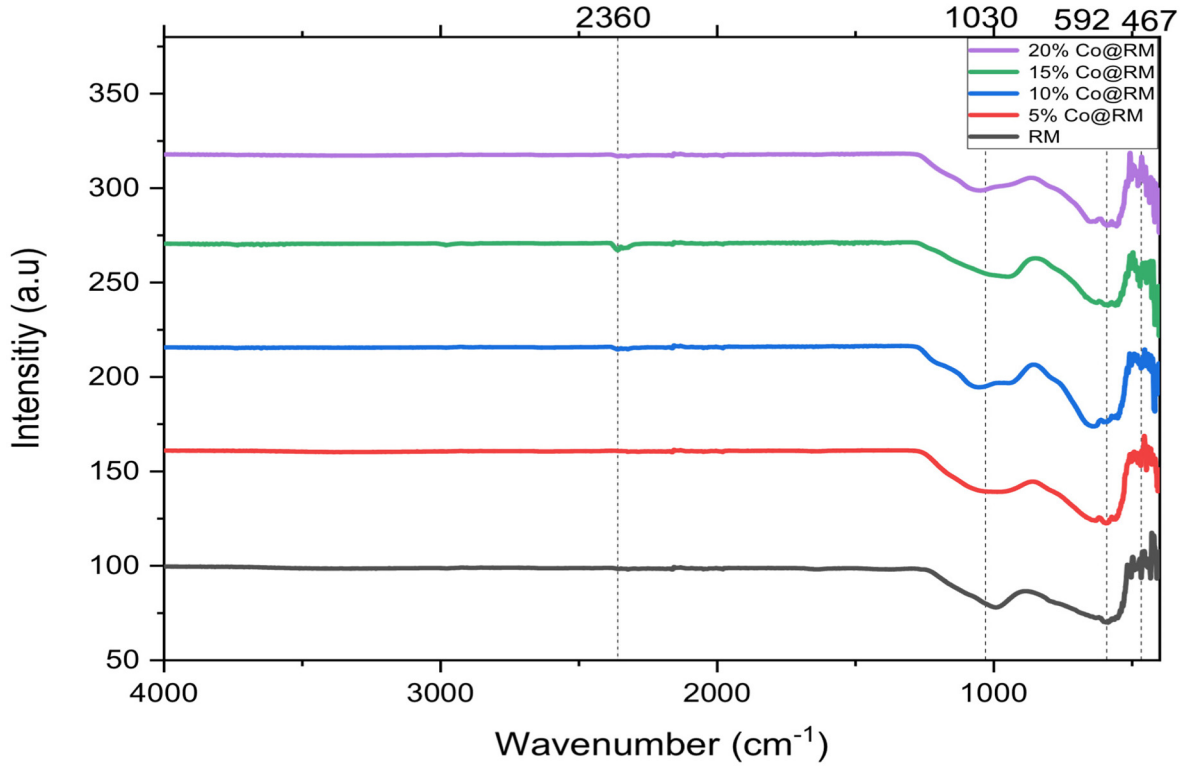

Figure 2. FT-IR spectra of RM and Co@RM (5, 10, 15, and 20%) catalysts

The FTIR spectra of the RM and the Co@RM (5–20 wt.%) catalysts had similar general patterns; thus, the Co loading had no significant effect on the general structure of the RM (Figure 2). A broad peak located at 998–1030 cm^{-1} was attributed to calcium silicate phases; these are associated with Si–O vibrations within the silicate framework[29]. The presence of silicate species was further supported by the band observed at ~460 cm^{-1}; this was assigned to Si–O stretching vibrations of quartz. The negligible shift in these bands with increasing Co content suggests that the silicate structure of the RM was largely preserved after Co loading. In the lower-wavenumber region (<700 cm^{-1}), the spectra were dominated by metal–oxygen vibrations, which were associated with the oxide components of RM. Notably, the band centered at 500–600 cm^{-1} became more pronounced with higher Co loading; this change can be attributed to the contribution of the Co–O vibrations from the cobalt-oxide species, in addition to the overlapping Fe–O modes inherently present in RM. Furthermore, the band observed at 460–470 cm^{-1} was assigned to Fe–O and Al–O bending vibrations[30,31]. The variation in intensity within this region suggests the incorporation of Co species within the oxide matrix, possibly in the form of highly dispersed Co oxides or mixed Co–Fe oxide phases.

Overall, no new bands were apparent in the high-wavenumber region, which suggests that the Co incorporation occurred primarily via interactions with existing oxygen sites. The gradual enhancement of the metal–oxygen vibration band supports the successful dispersion of the Co species on the RM surface without major structural modifications to the support.

The field emission scanning electron microscope (FESEM) images in Figure 3 show the morphologies of the Co@RM (0–20%) samples. The raw RM (Figure 3 (a)) possessed large irregular agglomerates with a porous structure. After Co incorporation,

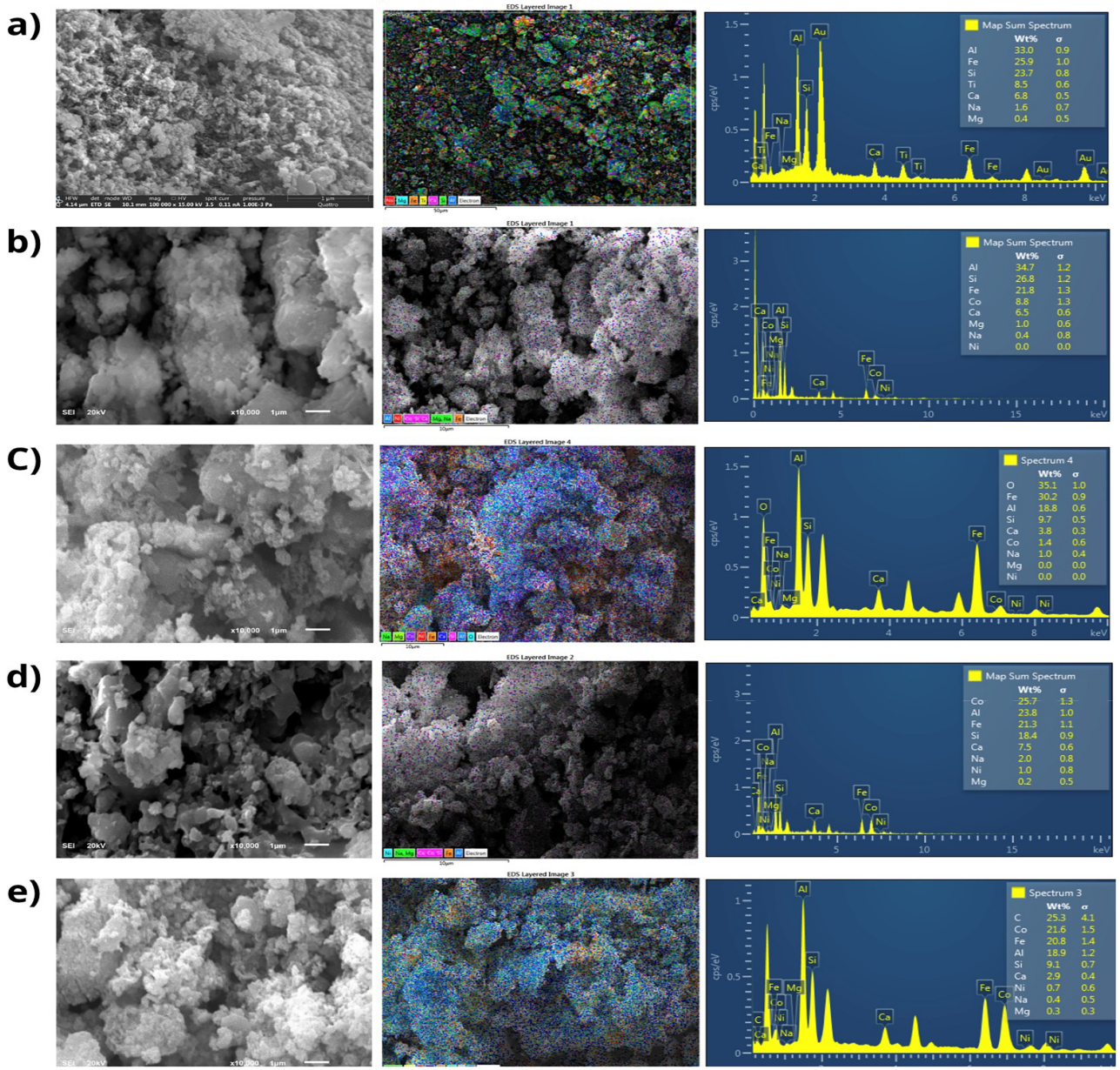

Figure 3. FESEM micrographs of (a) RM, (b) 5% Co@RM, (c) 10% Co@RM, (d) 15% Co@RM, and (e) 20% Co@RM catalysts and corresponding EDS analysis results

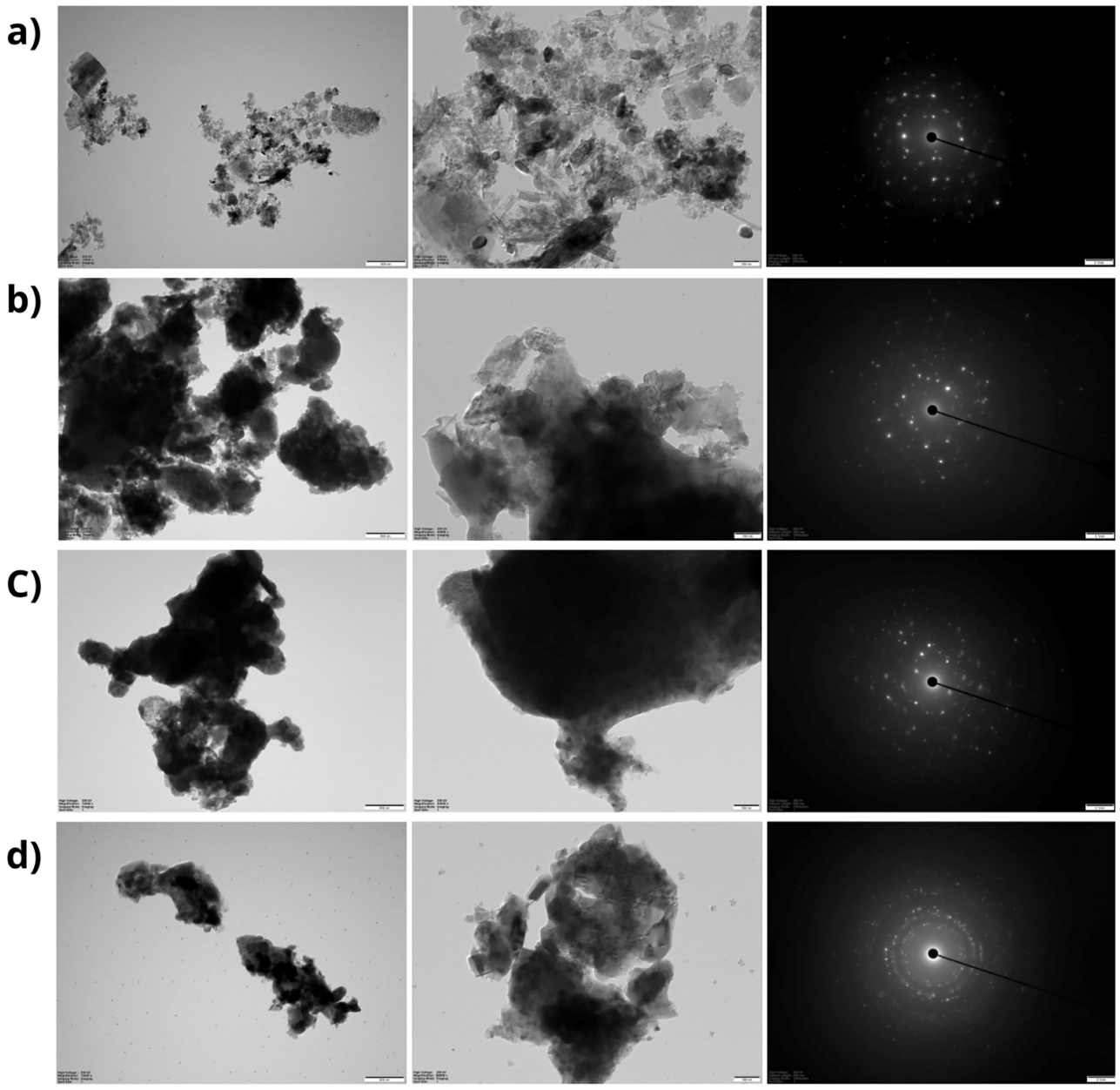

Figure 4. TEM results for Co@RM: (a) 5% Co-RM, (b) 10% Co-RM, (c) 15% Co-RM, and (d) 20% Co-RM

the morphology changed notably, with smaller and more dispersed particles appearing on the surface (Figures 3 (b)–(d)). With increased Co loading, the particles became more compact and less porous, indicating surface coverage by Co species. Energy-dispersive X-ray spectroscopy (EDS) analysis was conducted to assess the presence of Al, Si, Fe, Ca, Co, Na, and Mg in the Co@RM samples. The Co peaks increased with increasing loading, indicating the successful incorporation of Co on the RM surface.

The TEM micrographs of the Co@RM catalysts with different Co loadings (5–20%) are presented in Figure 4. The images were obtained at different magnifications (scales of 500, 100, and 21 nm are indicated in the figure). At low magnification, irregular agglomerated particles and heterogeneous morphologies were observed for all samples. The particles appeared as clustered nanodomains that aggregated into larger assemblies, indicating strong interparticle interactions within the matrix. As the Co content increased, the aggregates became denser and more compact, suggesting a progressive structural modification induced by the Co incorporation. Higher-magnification observations revealed fine nanocrystalline regions distributed throughout the RM framework. The increased contrast and clearer particle boundaries observed at higher Co loadings suggest the growth of Co-containing crystalline domains. The diffraction patterns recorded from the selected regions indicate a set of well-defined concentric rings and, thus, confirm the polycrystalline nature of the materials. Overall, the TEM results showed that the RM structure was not distorted by the presence of the Co, and that the crystallinity became more pronounced as the Co loading increased.

TGA was performed for different Co loadings (0–20%) to evaluate the thermal stabilities of the prepared catalysts as shown

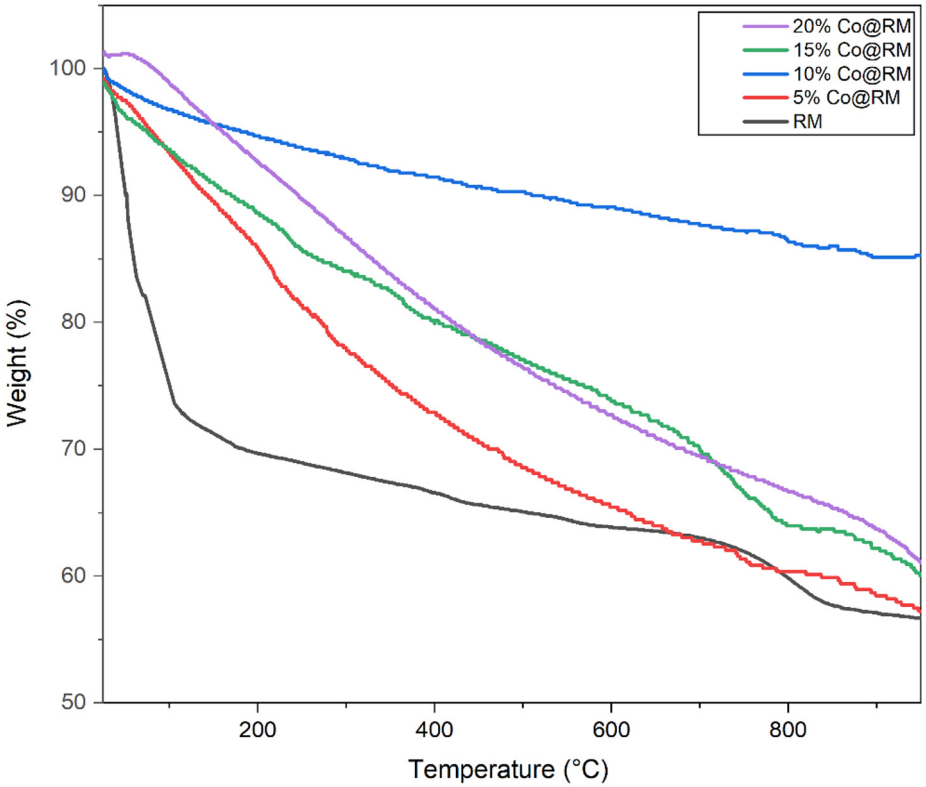

Figure 5. TGA results for RM and Co@RM (5, 10, 15, and 20%) catalysts

in Figure 5. A comparison of the TGA profiles revealed that the 10% Co@RM catalyst had the highest thermal stability; this was due to its lower total weight loss and the fact that it possessed the highest decomposition onset temperature. By contrast, the lowest thermal stability was observed for the RM, with higher weight loss in lower temperature ranges. The 10% Co@RM was deemed to have the optimal loading, as an effective balance between Co-particle dispersion and thermal stability without agglomeration was achieved. At low loadings (5% Co@RM), the stabilization was less effective as there were insufficient active sites. At high loadings (15% and 20% Co@RM), the Co efficacy in strengthening the structure may have been diminished by the formation of particle agglomerates.

3.2. Catalyst Activity of Steam Methane Reforming.

SMR is an endothermic process in which CH_4 reacts with steam (H_2O) to produce H_2 and CO. This reaction is usually performed at elevated temperatures and is the most efficient and mature industrial process for mass hydrogen production[32,33]. The main reaction is followed by the water–gas shift reaction, where CO and H_2O react together to yield H_2 and CO_2. Notably, the activity, stability, and deactivation resistance of the catalyst under severe reaction conditions critically impact the overall SMR performance.

Here, the gas products were analyzed online using a gas chromatograph equipped with a thermal conductivity detector (TCD) and flame ionization detector (FID). H_2, CO, and CO_2 were detected and quantified using the TCD, and the hydrocarbon compounds were analyzed using the FID. The gaseous products were separated on suitable columns (e.g., molecular sieves and Porapak columns) with an inert carrier gas (e.g., He or N_2). To ensure measurement reliability, all components were quantified using an external calibration method with known standard gas mixtures. The methane conversion rate and product selectivity were calculated from the measured flow rates as shown in Eqs. 3 and 4.

$$X_{CH4}\,(\%) = \frac{F_{CH4,int} - F_{CH4,out}}{F_{CH4,int}} \tag{3}$$

$$S_i\,(\%) = \frac{Fi}{\sum_j Fj} \times 100 \tag{4}$$

Here, X_{CH4} is the methane conversion rate; S_i is the selectivity of product i; $F_{CH4,int}$ and $F_{CH4,out}$ are the methane inlet and outlet flow rates, respectively; F_i is the flow rate of product i; and $\sum_j Fj$ represents the total flow rate for all the detected products.

Among the Co@RM catalysts examined in this study, the 5% Co@RM sample (Figure 6 (a)) exhibited the highest initial hydrogen yield of 50%. Furthermore, a CH_4 conversion of 96.9% was achieved. A slow decrease in catalytic activity was noted after 3 h on stream; this behavior reflected catalyst deactivation (caused by partial coking) and sintering of the Co particles. Although the initial hydrogen production was high, the concentration of the residual CH_4 was relatively low, which further confirmed that the reforming activity was high for this Co loading. The CO_2 formation remained limited, suggesting that side reactions such as the water–gas shift were minimal at this stage. For the 10% Co@RM catalyst, the hydrogen yield was low; however, the CH_4 conversion increased to >99% and remained stable for more than 4 h on stream, with the potential to persist for

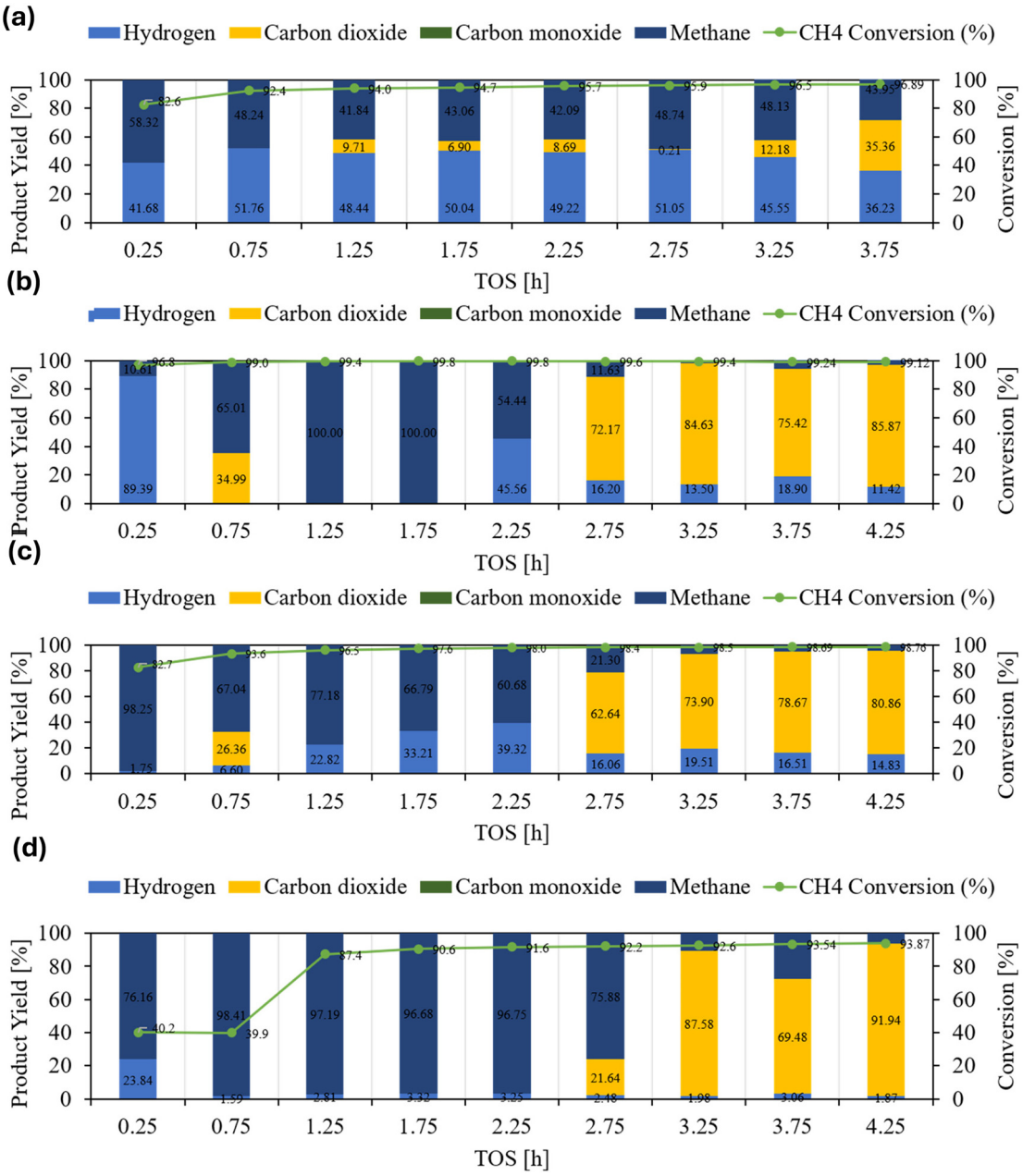

Figure 6. Performance analysis of steam methane reforming (SMR) for Co-RM catalysts: (a) 5% Co-RM, (b) 10% Co-RM, (c) 15% Co-RM, and (d) 20% Co-RM

even longer reaction times under extended testing. The conversion behavior was accompanied by an increase in the CO_2 yield, which indicated more active CH_4 activation. However, the H_2 selectivity was lower because the Co dispersion on the support was better and the number of active sites was increased.

The 15% Co@RM catalyst (Figure 6 (c)) exhibited performance comparable to the 10% sample, with similarly high CH_4 conversion levels and sustained catalytic activity. However, an additional increase in the CO_2 yield was detected, which suggests changes in the reaction routes or the influence of secondary reactions (e.g., the water–gas shift reaction). Furthermore, the methane activation remained efficient. At the maximum loading of 20% Co@RM (Figure 6 (d)), a drop in performance was clear. That is, both the CH_4 and CO_2 concentrations rose, reflecting lower efficiency and selectivity of the reforming process. This deactivation can be ascribed to sintering of the Co particles along with attenuation of the metal–support interactions, and, consequently, the number of active sites for CH_4 activation.

Overall, the catalytic performance of the Co@RM series observed in this study demonstrated that Co loading in a given catalyst critically determines the SMR activity, selectivity, and stability. The 5% Co@RM catalyst exhibited the highest hydrogen selectivity with moderate stability. The high hydrogen yield of the 5% Co@RM catalyst is ascribed to an optimal balance between active-site availability and initial resistance to carbon deposition. In contrast, the other catalysts experienced severe coking that covered the active sites, rendering them less efficient for catalyzing hydrogen production. However, increasing the loading to 10% yielded a remarkable improvement in stability and a significant increase in the methane conversion rate, revealing

a balance between dispersion and the number of active sites. For a further increase to 15%, a high conversion rate was maintained but undesired side reactions were promoted. These results indicate changes in the reaction pathway. A marked decrease in performance was observed for the 20% Co@RM sample; this can be attributed to particle agglomeration and diminishing metal–support interaction. Ultimately, the results show that intermediate Co loadings, particularly those of approximately 10–15%, provide the most favorable catalytic environment for efficient methane reforming. Moreover, sufficient active sites are available, good dispersion is maintained, and the deactivation phenomena are limited. Despite the promising performance of the Co@RM catalysts, this study has some limitations. The catalytic tests were conducted over a relatively short reaction time, and longer-term stability, catalyst regeneration, and detailed characterization of carbon deposition should be investigated in future work. The present findings are consistent with previous studies on Co-based steam methane reforming catalysts, which have reported that intermediate Co loadings provide the best balance between metal dispersion, methane conversion, and catalyst stability, whereas excessive Co loading promotes particle agglomeration, sintering, and catalyst deactivation.

4. CONCLUSION

This study investigated cobalt (Co, 5–20 wt.%) catalysts supported on RM for SMR. Structural and morphological analyses confirmed the successful incorporation of Co: Co oxides and Co–Fe mixed phases formed while the RM framework was preserved. Increasing the Co content enhanced the crystallinity but caused particle aggregation owing to the correspondingly stronger metal–support interactions. The catalytic performance was heavily dependent on the Co loading. A high initial hydrogen yield was obtained for the 5% Co@RM catalyst; however, this catalyst deactivated over time. The 10% Co@RM catalyst exhibited optimal performance, achieving a methane conversion rate exceeding 99% with stable long-term activity; this outcome was attributed to superior Co dispersion and abundant active sites. The 15% Co@RM catalyst maintained a high conversion rate but promoted CO_2 formation, indicating increased secondary reactions. At 20% loading, the activity declined as a result of particle agglomeration and blocked active sites. Overall, 10-wt.% Co was identified as the optimal loading to balance the catalyst dispersion, stability, and activity. The results highlight RM as a sustainable catalyst support for hydrogen production. The findings highlight the potential of red mud as a sustainable, low-cost catalyst support for hydrogen production via steam methane reforming. Future research should focus on long-term catalyst stability, regeneration, and optimization of reaction conditions to further improve catalytic performance.

AFFILIATIONS AND AUTHOR DETAILS

Undergraduate Author

Dana Alkhalifah – *Department of Mechanical Engineering, King Fahd University of Petroleum & Minerals, Dhahran 31261, Saudi Arabia*; 0009-0003-7074-3838
Email: s202359010@kfupm.edu.sa

Corresponding Author

Aasif Helal – *Research Mentor, Interdisciplinary Research Center for Hydrogen and Energy Storage, King Fahd University of Petroleum & Minerals, Dhahran 31261, Saudi Arabia*; 0000-0003-2013-5327
Email: aasifh@kfupm.edu.sa

ACKNOWLEDGEMENTS

The authors acknowledge the support provided by the Interdisciplinary Research Center for Hydrogen Technologies and Carbon Management (IRC-HTCM) at the King Fahd University of Petroleum and Minerals. The authors also extend their appreciation to the technical staff and laboratory team for their assistance with specimen preparation and testing.

REFERENCES

(1) Tolga Balta, M., Dincer, I. & Hepbasli, A. Thermodynamic assessment of geothermal energy use in hydrogen production. Int J Hydrogen Energy 34, 2925–2939 (2009).

(2) Abe, J. O., Popoola, A. P. I., Ajenifuja, E. & Popoola, O. M. Hydrogen energy, economy and storage: Review and recommendation. Int J Hydrogen Energy 44, 15072–15086 (2019).

(3) Esposito, D. V. Membraneless electrolyzers for low-cost hydrogen production in a renewable energy future. Joule 1, 651–658 (2017).

(4) Saidi, M. & Moradi, P. Conversion of biodiesel synthesis waste to hydrogen in membrane reactor: Theoretical study of glycerol steam reforming. Int J Hydrogen Energy 45, 8715–8726 (2020).

(5) Itoh, N., Kikuchi, Y., Furusawa, T. & Sato, T. Tube-wall catalytic membrane reactor for hydrogen production by low-temperature ammonia decomposition. Int J Hydrogen Energy 46, 20257–20265 (2021).

(6) Ganguli, A. & Bhatt, V. Hydrogen production using advanced reactors by steam methane reforming: A review. Frontiers in Thermal Engineering 3, 1143987 (2023).

(7) Abdin, Z. et al. Hydrogen as an energy vector. Renewable and Sustainable Energy Reviews 120, 109620 (2020).

(8) Song, H., Liu, Y., Bian, H., Shen, M. & Lin, X. Energy, environment, and economic analyses on a novel hydrogen production method by electrified steam methane reforming with renewable energy accommodation. Energy Conversion and Management 258, 115513 (2022).

(9) Yusuf, B. O. et al. Recent advances in bimetallic catalysts for methane steam reforming in hydrogen production: current trends, challenges, and future prospects. Chemistry–An Asian Journal 19, e202300641 (2024).

(10) Phanawadee, P. et al. Estimation of the remaining lifetime of deactivated catalyst via the spatial average catalyst activity illustrated by the water–gas shift and steam methane reforming processes. Reaction Kinetics, Mechanisms and Catalysis 121, 371–385 (2017).

(11) Argyle, M. D. & Bartholomew, C. H. Heterogeneous catalyst deactivation and regeneration: a review. Catalysts 5, 145–269 (2015).

(12) Liu, Y., Naidu, R. & Ming, H. Red mud as an amendment for pollutants in solid and liquid phases. Geoderma 163, 1–12 (2011).

(13) Bao, J. et al. Evaluating the effect of inert supports and alkali sodium on the performance of red mud oxygen carrier in chemical looping combustion. Ind Eng Chem Res 55, 8046–8057 (2016).

(14) Hossain Bhuiyan, M. M. & Siddique, Z. Hydrogen as an alternative fuel: A comprehensive review of challenges and opportunities in production, storage, and transportation. Int J Hydrogen Energy 102, 1026–1044 (2025).

(15) Dincer, I. & Acar, C. Review and evaluation of hydrogen production methods for better sustainability. Int J Hydrogen Energy 40, 11094–11111 (2015).

(16) Ighalo, J. O. & Amama, P. B. Recent advances in the catalysis of steam reforming of methane (SRM). Int J Hydrogen Energy 51, 688–700 (2024).

(17) Baharudin, L., Rahmat, N., Othman, N. H., Shah, N. & Syed-Hassan, S. S. A. Formation, control, and elimination of carbon on Ni-based catalyst during CO_2 and CH_4 conversion via dry reforming process: A review. Journal of CO_2 Utilization 61, 102050 (2022).

(18) Abdel-Fatah, M. A. & Amin, A. Catalyst deactivation and regeneration during methane catalytic cracking over supported nickel catalysts. Int J Hydrogen Energy 137, 236–246 (2025).

(19) Wang, D. et al. Integrated process for partial oxidation of heavy oil and in-situ reduction of red mud. Applied Catalysis B: Environmental 258, 117944 (2019).

(20) Sushil, S. & Batra, V. S. Catalytic applications of red mud, an aluminium industry waste: A review. Applied Catalysis B: Environmental 81, 64–77 (2008).

(21) Hong, Q. et al. Evaluation of red mud as oxygen carrier for chemical looping combustion of methane and biomass in fluidized bed. Fuel Process Technol 222, 106964 (2021).

(22) Katheria, S., Gupta, A., Deo, G. & Kunzru, D. Effect of calcination temperature on stability and activity of Ni/MgAl2O4 catalyst for steam reforming of methane at high pressure condition. Int J Hydrogen Energy 41, 14123–14132 (2016).

(23) Alfuhaid, L. T., Nasser, G. A., Alabdulhadi, R. A., Khan, M. Y., Yamani, Z. H. & Helal, A. Steam reforming of dodecane using Ni-red mud catalyst: A sustainable approach for hydrogen production. 86, 177–184 (2024).

(24) Jihar, K., Barrio, V. L., Kirm, I., Benzaouak, A. & Bouziane, K. Effect of Cobalt–Nickel ratio on the acid-base properties of Co–Ni/TiO2 catalysts via TPR and TPD analysis for steam reforming hydrogen production. Int J Hydrogen Energy 152, 150062 (2025).

(25) Chen, H. et al. Cobalt-doped red mud composite as a porous catalyst for activating peroxymonosulfate to degrade methylene blue. Environ. Res. 293, 123793 (2026).

(26) Siang, T. J. et al. Hydrogen production from CH_4 dry reforming over bimetallic Ni–Co/Al2O3 catalyst. Journal of the Energy Institute 91, 683–694 (2018).

(27) Argyle, M. D. & Bartholomew, C. H. Heterogeneous catalyst deactivation and regeneration: a review. Catalysts 5, 145–269 (2015).

(28) Dawood, F., Anda, M. & Shafiullah, G. M. Hydrogen production for energy: An overview. Int J Hydrogen Energy 45, 3847–3869 (2020).

(29) Hu, Z., Zhao, H. & Gao, Z. High-surface-area activated red mud supported Co_3O_4 catalysts for efficient catalytic oxidation of CO. RSC Adv 6 (97): 94748–94755. (2016).

(30) Singh, S. et al. Role of iron in the enhanced reactivity of pulverized Red mud: Analysis by Mössbauer spectroscopy and FTIR spectroscopy. Case Studies in Construction Materials 11, e00266 (2019).

(31) He, Y. et al. A novel red mud-based Co_3 O_4–Fe_2 O_3–Co_2 AlO_4 composite as a peroxymonosulfate activator for effective degradation of lomefloxacin hydrochloride. New Journal of Chemistry 48, 15687–15703 (2024).

(32) Ganguli, A. & Bhatt, V. Hydrogen production using advanced reactors by steam methane reforming: A review. Frontiers in Thermal Engineering 3, 1143987 (2023).

(33) Bengaard, H. S. et al. Steam Reforming and Graphite Formation on Ni Catalysts. Journal of Catalysis 209, 365–384 (2002).